INSTITUTE OF PHYSICS PUBLISHING PHYSICS IN MEDICINE AND BIOLOGY

Phys. Med. Biol. **50** (2005) 387–397 doi:10.1088/0031-9155/50/2/015

Radial and temporal variations in surface heat transfer during cryogen spray cooling

Walfre Franco[1,3], Jie Liu[1], Guo-Xiang Wang[2], J Stuart Nelson[3] and Guillermo Aguilar[1,3]

[1] Department of Mechanical Engineering, University of California, Riverside, CA 92521, USA
[2] Department of Mechanical Engineering, University of Akron, Akron, OH 44325, USA
[3] Beckman Laser Institute, University of California, Irvine, CA 92617, USA

Received 12 August 2004, in final form 7 November 2004
Published 5 January 2005
Online at stacks.iop.org/PMB/50/387

Abstract

Cryogen spray cooling (CSC) is a heat extraction process that protects the epidermis from thermal damage during dermatologic laser surgery. The objective of the present work is to investigate radial and temporal variations in the heat transferred through the surface of a skin phantom during CSC. A fast-response thermal sensor is used to measure surface temperatures every 1 mm across a 16 mm diameter of the sprayed surface of the phantom. An analytical expression based on Fourier's law and Duhamel's theorem is used to compute surface heat fluxes from temperature measurements. Results show that radial and temporal variations of the boundary conditions have a strong influence on the homogeneity of heat extraction from the skin phantom. However, there is a subregion of uniform cooling whose size is time dependent. It is also observed that the surface heat flux undergoes a marked dynamic variation, with a maximum heat flux occurring at the centre of the sprayed surface early in the spurt followed by a quick decrease. The study shows that radial and temporal variations of boundary conditions must be taken into account and ideally controlled to guarantee uniform protection during CSC of human skin.

Introduction

CSC is essential to laser dermatologic and cosmetic surgery. Its purpose is to protect the epidermis from excessive heating induced by unintended melanin absorption of laser light (Nelson *et al* 1995). Heat extraction from skin during CSC is a function of many fundamental spray parameters, such as average droplet diameter and velocity, mass flow rate, temperature and spray density, among others (Aguilar *et al* 2001, Karapetian 2002), that vary in time and space within the spray cone. Therefore, heat extraction from human skin during CSC-assisted laser surgery is non-uniform (Franco *et al* 2004a, 2004b). There are only a few investigations that address lateral variations in heat transfer during CSC. Verkruysse *et al* (1999) investigated

Table 1. Thermal properties of epidermis (Duck 1990) and sensor components (Incropera and Dewitt 1996, http://www.matweb.com).

	Epidermis	Plexiglas®	Al foil	Scotch tape®
c (J kg^{-1} K^{-1})	3600	1300–1500	896	1400
ρ (kg m^{-3})	1200	1150–1190	2710	1280
k (W m^{-1} K^{-1})	0.21	0.19–0.24	205	0.22
α (m^2 s^{-1})	$\approx 0.5 \times 10^{-7}$	$\approx 1.3 \times 10^{-7}$	$\approx 8.4 \times 10^{-5}$	$\approx 1.2 \times 10^{-7}$

how the delivery nozzle design influences the cooling rate of CSC. They recorded interior temperatures—at different depths within an epoxy substrate—along and 3 mm apart from the spray axis during CSC. The authors observed different temperature evolutions in time for these radial locations and suggested that the heat transfer coefficient h and cryogen temperature are not the same throughout the sprayed area. Aguilar *et al* (2001) used a linear array of eight thermocouples to measure steady-state lateral variations in spray temperature. Their results showed that the temperature of the spray is practically constant (≈ -58 °C) within a 6 mm radius. Choi and Welch (2002) imaged changes in radiation on the back side of an aluminium sheet (0.8 mm thick) to determine front side two-dimensional distributions of surface temperature during CSC. The authors found a nearly Gaussian shape in the surface temperature distribution and, that by assuming uniform boundary conditions, cooling is overestimated at radii greater than 2.5 mm. In this investigation a skin phantom with thermal properties similar to those of human skin is used as a substrate to determine radial and temporal variations in surface heat transfer during CSC.

Experimental and numerical methods

Spray cooling system

Refrigerant hydrofluorocarbon 134a (Suva® 134a, Dupont, Wilmington DE), with a boiling temperature $\theta_b \approx -26$ °C at atmospheric pressure, is kept at a saturation pressure of 600 kPa at 22.5 °C and delivered to a fuel injector attached to a straight-tube nozzle. The stainless steel nozzle has an inner diameter $d = 0.7$ mm and length $l = 32$ mm. The chosen d is similar to that of commercial devices currently used to treat patients. The spray system is electronically controlled and set to deliver single 60 ms cryogen spurts.

Fast-response temperature sensor

The thermal sensor is schematically shown in figure 1(a). A miniature type-K thermocouple (CHAL-001, Omega, Stamford CT) is placed on top of a 6 mm thick bar of polymethyl methacrylate (Plexiglas®). A 0.5 mm thick layer of cellulose tape (Scotch tape®) is placed next to the thermocouple bead. The bead and tape are covered by aluminium foil (surface 15×10 mm and thickness $L = 0.02$ mm). Thermal paste is used around the thermocouple bead to ensure good thermal contact. The sensor—similar to that described by Aguilar *et al* (2003)—provides a substrate with skin-like thermal properties and has a response time of the order of milliseconds: the thermal diffusion time of the foil is $\approx$5 ms (as described in the heat transfer calculations subsection), and the bead time constant is $\approx$2 ms (according to the manufacturer). Thermal properties of the epidermis and sensor components can be found in table 1.

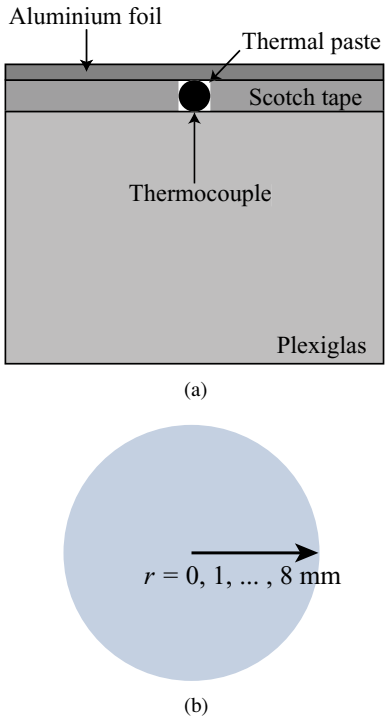

Figure 1. (a) Fast-response temperature sensor. (b) Measurements across the sprayed surface.

Temperature is acquired through an A/D converter (instruNet, GW Instruments Inc., Sommerville MA) hardware and LabView software (National Instruments, Austin TX) at 2000 Hz, and noise is filtered out by averaging 30 adjacent points—the number of points was determined by comparison to original data avoiding to exclude significant curve features. The sensor has an initial temperature of 22.5 °C and is placed 40 mm away from the nozzle tip. Initially, the thermocouple bead is placed at the centre of the spray cone and, subsequently, displaced radially, using a BiSlide® positioning system (Velmex Inc., Bloomfield NY), to measure temperatures every 1 mm from the centre, $r = 0$ mm, to the periphery of the sprayed surface, $r = 8$ mm—see figure 1(b). This is done in two opposite directions, such that data are acquired along the entire 16 mm diameter of the spray cone. A separate spray is applied for every lateral displacement. Repeatability of measurements is shown in the results and discussion section.

Heat transfer calculations

For many laser therapies assisted by CSC the width of the sprayed skin area is of the order of 20 mm, the time scale is in milliseconds (e.g., typical CSC spurt durations, delay time and laser pulse during port wine stains (PWS) therapy range from 60–100 ms, 30–40 ms and 0.5–2 ms, respectively, thus duration of therapy is less than 150 ms), and the depth of interest is ≈0.5 mm (epidermal thickness is ≈50 μm and targeted blood vessels are embedded in dermis within 500 μm depth). Therefore, time, depth and lateral scales allow heat transfer to be modelled as a one-dimensional heat diffusion problem with known surface temperature.

The material thermal diffusivity, α, is defined as the ratio of thermal conductivity, k, to density, ρ, and specific heat, c, i.e., $\alpha = k/(\rho c)$. For the aluminium foil, the thermal diffusion time is $L^2/\alpha \approx 5 \times 10^{-6}$ s, and the Biot number (Incropera and Dewitt 1996), hL/k, for a typical heat transfer coefficient of spray, $h \simeq 10\,000\ \mathrm{W\,m^{-2}\,K^{-1}}$ (Incropera and Dewitt 1996), is $\approx 1 \times 10^{-3}$. Since $Bi \ll 1$, the temperature of the foil is assumed to be spatially uniform in the vicinity of the thermocouple bead. It follows that the thermocouple measures point surface temperatures. To verify this assumption, a finite element method (Femlab, Comsol Inc., Burlington MA) is used to solve for two-dimensional heat diffusion within a Plexiglas® substrate covered by aluminium foil. In this simulation, dynamic and radial measurements of surface temperature—presented in the results section—are used as boundary condition. In particular, for CSC-assisted dermatologic laser surgery, the bioheat transfer or Pennes equation (Pennes 1948) reduces to the classic heat diffusion equation since the heat conveyed by blood perfusion and generated by body metabolism is negligible because of the time scales relevant to the therapy (van Gemert and Welch 1989). If the surface temperature is known, a direct heat conduction problem for the temperature distribution within the substrate may be solved to determine the temperature gradient at the surface and, subsequently, the surface heat flux from Fourier's law. Alternatively, Duhamel's theorem can be used to evaluate the temperature gradient at the surface if thermal properties remain constant. Both methods provide nearly identical solutions; however, the latter is used herein since it is easier to implement numerically.

Duhamel's theorem is based on the principle of superposition and states that the substrate thermal response at t equals the total sum of what the substrate experienced in small steps prior to t (Carslaw and Jaeger 1959, Özişik 1980, Beck *et al* 1985). For constant thermal properties, the temperature form of Duhamel's theorem is

$$\theta(z,t) = \theta_0 + \int_{t_0}^{t} u(z, t-\tau)\frac{\mathrm{d}T}{\mathrm{d}\tau}\,\mathrm{d}\tau, \tag{1}$$

where θ is the substrate temperature, θ_0 is the uniform initial temperature, u is the temperature response function of the substrate (initially at zero temperature) to a unit step in surface temperature, z is the coordinate perpendicular to the surface, $t - \tau$ is the time that has elapsed since the step at τ, and T is the surface temperature (Carslaw and Jaeger 1959, Meyers 1971). Using equation (1), Fourier's law (Incropera and Dewitt 1996), for a continuous surface temperature in time, can be written as

$$q(t) = -k\left.\frac{\partial\theta}{\partial z}\right|_{z=0}, \tag{2}$$

$$= -k\int_{t_0}^{t}\left.\frac{\partial u(z,t-\tau)}{\partial z}\right|_{z=0}\frac{\mathrm{d}T}{\mathrm{d}\tau}\,\mathrm{d}\tau, \tag{3}$$

where partial derivatives are evaluated at the surface. The unit step function for a semi-infinite planar solid is (Özişik 1980, Beck *et al* 1985)

$$u(z,t) = 1 - \mathrm{erf}\left(\frac{z}{2\sqrt{\alpha t}}\right), \tag{4}$$

then

$$\partial u/\partial z = -1/\sqrt{\pi\alpha t}. \tag{5}$$

Substituting equation (5) into (3), the surface heat flux, $q(t)$, can be written as

$$q(t) = \sqrt{\frac{k\rho c}{\pi}}\int_{t_0}^{t}\frac{1}{\sqrt{t-\tau}}\frac{\mathrm{d}T}{\mathrm{d}\tau}\,\mathrm{d}\tau. \tag{6}$$

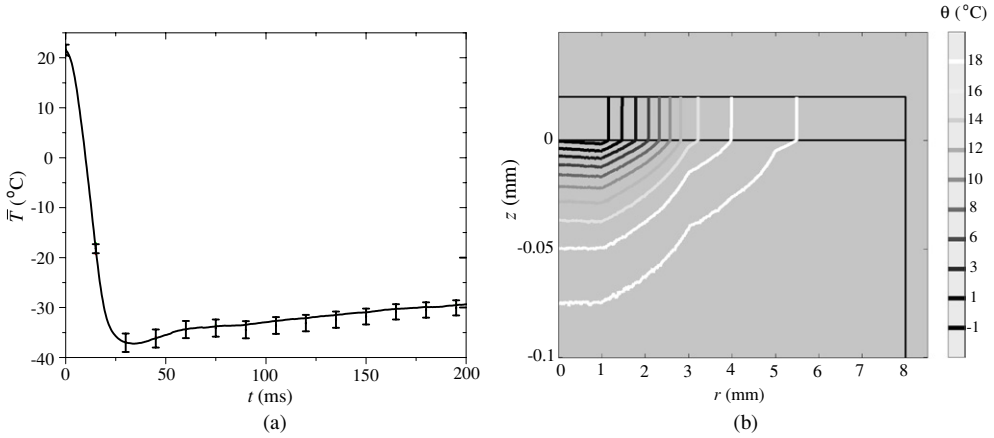

Figure 2. (a) Average temperatures for $r = 0$ mm. The bars denote standard deviations. (b) Isotherms within aluminium and Plexiglas® at $t = 100$ ms for radial and time-dependent boundary conditions.

Assuming that the surface temperature is measured at discrete times t_i and that the surface temperature varies linearly in time between successive times, equation (6) can be integrated analytically—see the appendix—to obtain

$$\hat{q}_I = 2\sqrt{\frac{k\rho c}{\pi}} \sum_{i=1}^{I} \left(\frac{T_i - T_{i-1}}{t_i - t_{i-1}} \right) (\sqrt{t_I - t_{i-1}} - \sqrt{t_I - t_i}), \tag{7}$$

$$= 2\sqrt{\frac{k\rho c}{\pi}} \sum_{i=1}^{I} \frac{T_i - T_{i-1}}{\sqrt{t_I - t_i} + \sqrt{t_I - t_{i-1}}}, \tag{8}$$

where $\hat{q}$ is the approximate surface heat flux for a semi-infinite planar body. A more detailed discussion about this approximation can be found in (Beck *et al* 1985). For simplicity, $\hat{q}$ is written as q in the following sections.

Results and discussion

Repeatability of experiments and verification of the one-dimensional approximation are presented in figure 2. The average values, $\overline{T}$, of four independent measurements at the centre of the sprayed area are shown in figure 2(a); the error bars denote standard deviations. Similar curves were obtained for each location. Repeatability of the thermal history shows that the spray system is very stable. Isothermal curves within a Plexiglas® substrate and a 0.02 mm aluminium foil cover at $t = 100$ ms are presented in figure 2(b). Isotherms within the aluminium foil are straight vertical lines, thus, the thermocouple measures local surface temperatures.

Temporal evolution of heat transfer

Dynamics of surface temperature, T, and heat flux, q, along the sprayed surface radius are shown in figures 3(a) and (b), respectively. Minimum surface temperature, $T_{\min}$, and maximum surface heat flux, $q_{\max}$, occur at different times at each radial location. Also in figure 3(a), the slopes of curves during cooling illustrate that locations closer to the centre of the spray

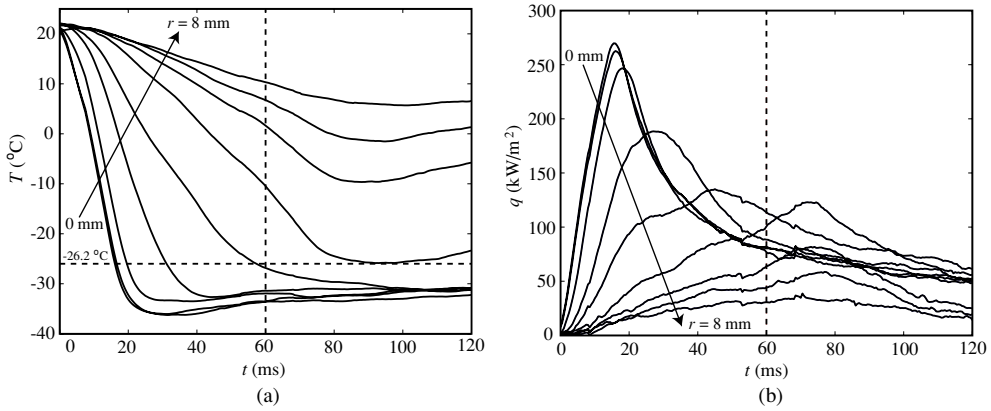

Figure 3. Dynamics of surface (a) temperature and (b) heat flux. Vertical and horizontal dashed lines denote ends of cryogen spurt and cryogen boiling temperature, respectively.

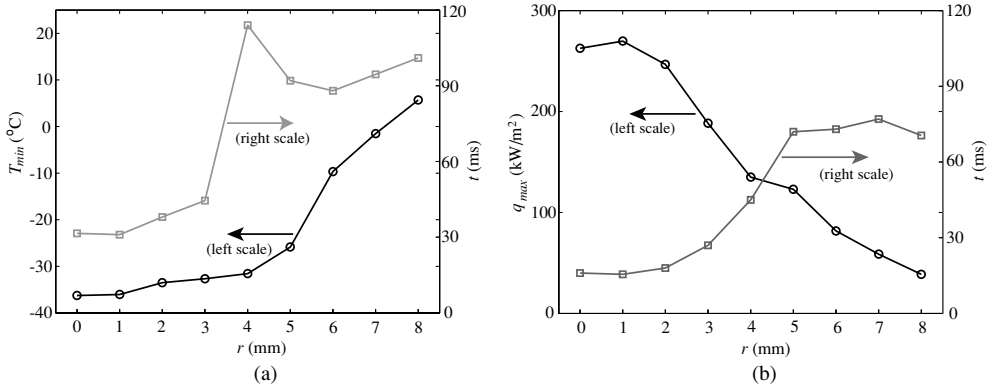

Figure 4. Times of occurrence (□ right scale) and magnitudes of (a) $T_{\min}$ (○ left scale) and (b) $q_{\max}$ (○ left scale) along radial direction.

undergo a higher rate of change of T, thus heat extraction is faster. A separation of curves is evident during and after the spurt; there is a set of locations that show similar $T(t)$ values which corresponds to the grouped curves at the bottom of figure 3(a), i.e., $r = 0$, 1 and 2 mm. This is also true for $q(t)$ in figure 3(b). It follows that there is an inner region of radial uniform cooling within the sprayed surface.

$T_{\min}$ and times of occurrence as a function of position are plotted in figure 4(a). The lowest $T_{\min}$ occurs early in the spurt (≈30 ms) by the spray axis; however, these values are similar to those at $r = 1$ and 2 mm. Local $q_{\max}$ and times of occurrence as a function of radial position are plotted in figure 4(b). The highest $q_{\max}$ rises early in the spurt (≈15 ms) at $r = 1$ mm, this value is quite similar to those by the spray axis and $r = 2$ mm, and times of occurrence are nearly identical. It seems that within a 2 mm radius the spray is homogeneous. Note that although $r = 3$ and 4 show similar $T_{\min}$ to those for $r \leqslant 2$, its dynamics are not: $T_{\min}$ occurs later, figure 3(a), and cooling rates are lower, figure 3(b).

Differences in temperature, $\Delta T(r, t)$, and heat flux, $\Delta q(r, t)$, are used to assess the uniformity of cooling conditions at the sprayed surface. $\Delta T_{i,j}$ is defined as the difference in temperature between the centre of the sprayed area and radial location j at time instant i, that

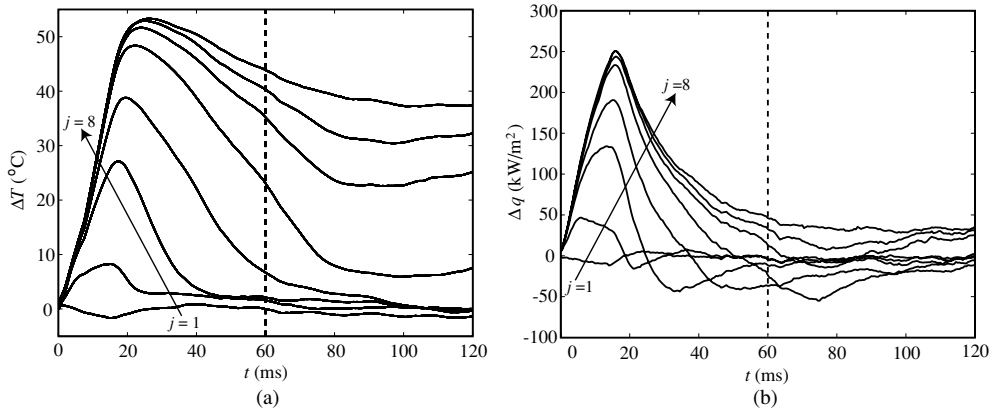

Figure 5. Dynamics of differences in (a) temperature and (b) heat flux between the centre of the spray surface and at other locations. Dashed line denotes end of cryogen spurt.

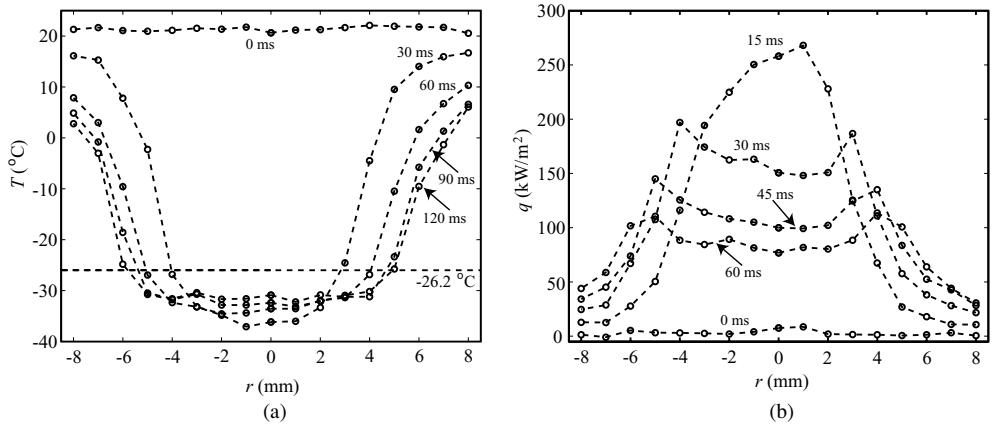

Figure 6. Radial distributions of surface (a) temperature and (b) heat flux along the sprayed surface diameter. Horizontal line represents cryogen boiling temperature.

is $\Delta T_{i,j} = T_{i,0} - T_{i,j}$, where $j = 1, 2, \ldots, 8$. Similarly, the difference in heat flux, $\Delta q_{i,j}$, is defined as $\Delta q_{i,j} = q_{i,0} - q_{i,j}$. Temporal variations of ΔT and Δq are shown in figure 5. In figure 5(a), ΔT_j increases over time, achieves a maximum and then decreases. The largest difference in surface temperature between the spray axis and periphery is more than 50 °C and occurs during the spurt, $t \approx 25$ ms. Subsequently, ΔT_j decreases but its magnitude is still significant at peripheral locations: at $t = 120$ ms, $\Delta T_8 \approx 38$ °C. In figure 5(b), the largest difference in surface heat flux is 250 kW m^{-2}, and Δq_j becomes negative when heat fluxes at peripheral locations are larger than that at the centre, as shown in the next section and figure 3(b).

Radial evolution of heat transfer

Radial distributions of T and q at specific time intervals are shown in figure 6. Initially in figure 6(a), every location is at room temperature (first curve from top). Next, the spray cools down the skin phantom and temperature at every location decreases at different rates.

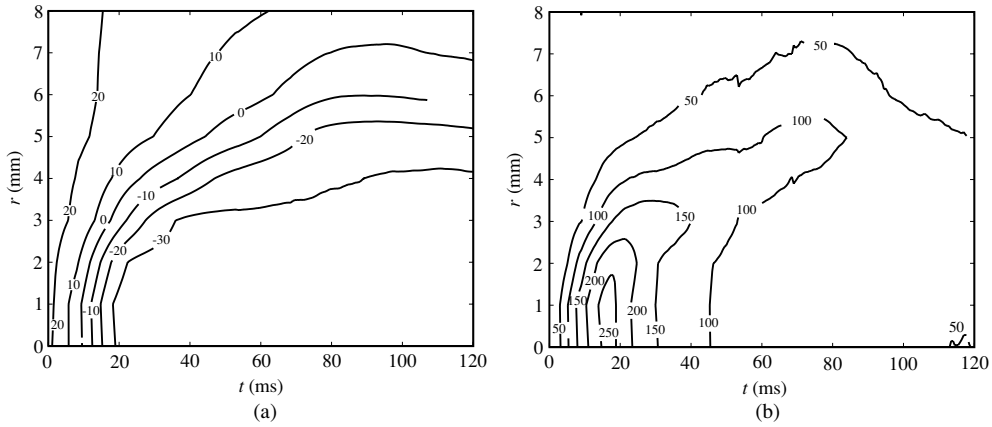

Figure 7. Time and space dependent surface (a) temperature and (b) heat flux profiles. Curves represent isotherms in °C and constant heat flux in kW m^{-2}, respectively.

The second curve ($t = 30$ ms) corresponds to the time when the lowest $T_{\min}$ occurs—see figure 4(a). The third curve corresponds to the end of the spurt ($t = 60$ ms). T distributions have a nearly Gaussian shape, which is in agreement with the results of Choi and Welch (2002). In figure 6(b), at $t = 0$ ms the skin phantom is in thermal equilibrium and there is no heat transfer. Upon spray impingement a heat flux from the phantom to the surrounding environment occurs. As shown in figure 4(b), the highest $q_{\max}$ occurs at $t \approx 15$ ms which corresponds to the curve with shape similar to a Gaussian distribution in figure 6(b). Next, q decreases at the centre of the spray but keeps rising near the periphery.

As shown, cooling is not uniform in either time or space. However, figures 6(a) and (b) illustrate that there is a subregion within the sprayed surface where cooling conditions are almost homogeneous. This subregion is defined by the radius for which temperature and heat flux values are similar and, thus, time dependent. Note in figure 6(a) that over time the radius of uniform T increases. For the spray system studied herein, cooling conditions are uniform within a 2 mm radius at any time, and for $90 \leqslant t \leqslant 120$ ms surface conditions are uniform within a 4 mm radius.

Temporal and radial evolution of heat transfer

The evolution in time and space of T and q are shown in figure 7. Isotherms in figure 7(a) show that the surface experiences a marked dynamic variation in temperature during the first 20 ms of the spurt: from 22.5 to −30 °C. The figure also shows that the closer the location is to the spray axis, the more remarkable are the temporal variations in temperature. This is also true for the surface heat flux: lines of constant q in figure 7(b) show that the overall maximum heat flux at the spray axis rises early in the spurt and, subsequently, there is a quick decrease in heat flux. Most of the heat extracted from the skin phantom occurs during the first 20 ms of the 60 ms cryogen spurt. It follows that CSC is a highly dynamic process with a time scale of 10^{-3} s and significant radial variations in a 10^{-3} m length scale.

Liquid cryogen pool

If T is below the boiling temperature θ_b of the impinging liquid cryogen droplets, then it is plausible that liquid cryogen is not evaporating completely at the solid–spray interface, but

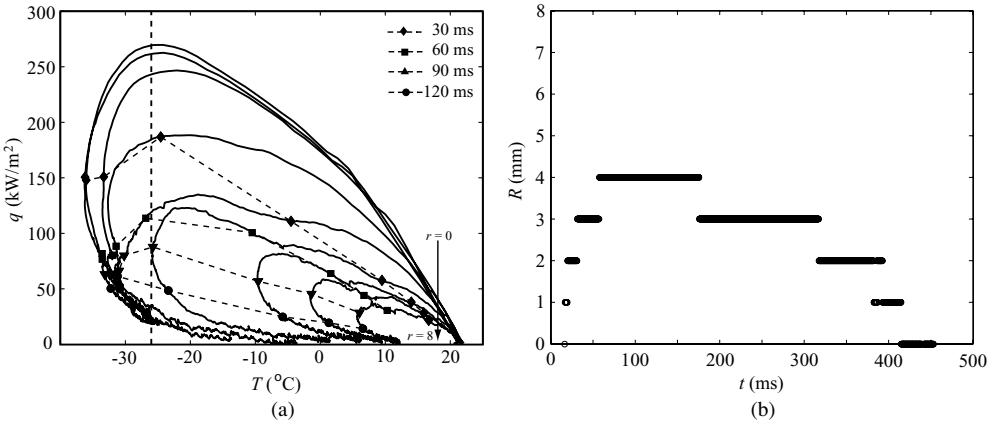

Figure 8. (a) Heat flux as a function of temperature; vertical dashed line denotes cryogen boiling temperature, symbols mark specific times, arrow indicates radial location. (b) R as a function of time.

rather accumulating. Aguilar *et al* (2003) defined the residence time, t_r, as the time interval for which $T \leqslant \theta_b$ under experimental conditions. They found that t_r changes as the spray system parameters—spurt duration, tube nozzle geometry, surface–nozzle distance—are varied. In this study, t_r also varies radially. q as a function of T for a time period of 500 ms is plotted in figure 8(a). T decreases and remains below θ_b for a significant period of time near the centre of the sprayed surface, while T is never close to θ_b at peripheral locations. It is clear that surface thermodynamics during CSC at the centre, middle and periphery of the spray are quite different. Figure 8(b) shows the time evolution of R which is defined as the radius where temperatures are below saturation values, i.e., $T < \theta_b$. If the latter inequality is assumed to be linked to a phase change, R can be interpreted as the radius of a cryogen pool that originates at the centre of the sprayed surface, expands and then shrinks as it disappears. Therefore, figure 8(b) shows that a cryogen pool of significant size is quite likely to exist during laser irradiation even if a delay between CSC and the laser pulse is introduced.

Discussion

Fluid mechanics and heat transfer of spray systems are highly complex. As shown, cooling conditions at the skin phantom boundary vary radially and temporally during and after the liquid cryogen spurt. The more uniform the temperature distribution at the surface, the more uniform interior temperatures are distributed. Therefore, epidermal protection provided by CSC prior to laser irradiation is non-uniform. However, figure 5 shows that there is a subregion where cooling conditions are relatively more homogeneous within the spray cone, hence a subregion of uniform epidermal protection can be identified, provided that the laser beam radius is smaller than or equal to that of the subregion cooling radius. The radius of uniform protection is time dependent, consequently the instant at which the laser pulse is supplied is critical as illustrated below. Surface temperature values are similar at 120 ms, figure 5(a), within a 4 mm radius, figure 6(a). Then, a 60 ms cryogen spurt and 60 ms delay prior to laser irradiation seem to be an appropriate time sequence for port wine stains (PWS) therapy. Nevertheless, CSC is intended to be a selective heat extraction process. It is possible that at 120 ms, the temperature of the targeted PWS blood vessels could unintentionally be reduced. It follows that more energy will be needed to reach the damage threshold of PWS blood vessels.

In a typical CSC-assisted dermatologic laser surgery scenario, the laser pulse is supplied either at the end of the cryogen spurt or 30 to 40 ms thereafter. The region of uniform heat transfer for a 60 ms spurt and no delay has an approximate radius of 3 mm, figure 6(a). It follows that a laser beam with a radius equal to or less than 3 mm would be appropriate. Common laser beam radius ranges from 1 to 5 mm. As the radius of the laser beam increases, if CSC is not adjusted—for example, by changing spurt duration or skin to nozzle distance—the probability of epidermal damage at the outside edge of the beam laser increases as well. Consequently, there is a critical relation between laser beam radius and subregion of uniform cooling. The effectiveness of CSC relies on its ability to produce high heat fluxes in short periods of time that allow selective cooling of the epidermis; however, marked heat transfer dynamics take place only by the spray axis.

Thermal histories in a 2 mm radius are quite similar, as illustrated in figures 7(a) and (b). Hence, numerical studies of CSC-assisted laser surgery that assume uniform radial boundary conditions may overestimate cooling at radii greater than 2 mm. Choi and Welch (2002) reported that by assuming uniform boundary conditions, cooling is overestimated at radii greater than 2.5 mm; however, their results are based on a simulation that used experimental measurements on a 0.8 mm thick aluminium foil as boundary conditions. Because of the aluminium thickness and the lack of substrate, it is possible that lateral heat conduction may have been significant and radial variations were overestimated due to the difference in thermal conductivities between the epidermis and aluminium—see table 1.

Conclusions

The heat extraction process at the surface during CSC is a complex temporal and spatial phenomenon. The difference in temperatures between different locations in the sprayed surface is significant, especially between central and peripheral locations. Closer to the centre, the dynamic thermal response is faster and lower temperatures are reached. The overall maximum heat flux, $q_{\max}$, occurs very early in the spurt at the centre of the sprayed surface. Epidermal protection provided by CSC is not uniform. However, there exists a subregion of uniform cooling conditions within the sprayed area and, consequently, a subregion of uniform epidermal protection. For $r = 2$ mm the temperature differences between the centre of the sprayed surface and locations within this area are less than 5 °C at any instant in time. Therefore, skin boundary conditions must be taken into account and controlled in order to guarantee uniform epidermal protection during CSC-assisted dermatologic laser surgery.

Acknowledgments

This work was supported in part by the National Institutes of Health (HD42057 to GA and AR47551 to JSN). Research support by Dr Julio C Ramírez-San-Juan is greatly appreciated.

Appendix

Let $\chi = \sqrt{k\rho c/\pi}$. Provided that $t_i - t_{i-1}$ is small, equation (6) can be approximated as

$$q^*(t_I) = \chi \sum_{i=1}^{I} \left(\frac{T_i - T_{i-1}}{t_i - t_{i-1}} \right) \frac{1}{\sqrt{t_I - t_i}} (t_i - t_{i-1}), \tag{A.1}$$

$$= \chi \sum_{i=1}^{I} \left(\frac{T_i - T_{i-1}}{t_i - t_{i-1}} \right) \frac{1}{\sqrt{t_I - t_i}} ((t_I - t_{i-1}) - (t_I - t_i)), \tag{A.2}$$

$$= \chi \sum_{i=1}^{I} \left(\frac{T_i - T_{i-1}}{t_i - t_{i-1}} \right) \frac{(\sqrt{t_I - t_{i-1}} - \sqrt{t_I - t_i})(\sqrt{t_I - t_{i-1}} + \sqrt{t_I - t_i})}{\sqrt{t_I - t_i}}. \tag{A.3}$$

Let $\sqrt{t_I - t_{i-1}} + \sqrt{t_I - t_i} = 2\sqrt{t_I - t_i} + \epsilon$, where ϵ is small compared to the other term. Equation (7) is obtained by substituting the last expression in equation (A.3) and neglecting the product of ϵ and the difference of square roots, such that $\hat{q} \approx q^*$.

References

Aguilar G, Majaron B, Pope K, Svaasand L O, Lavernia E J and Nelson J S 2001 Influence of nozzle-to-skin distance in cryogen spray cooling for dermatologic laser surgery *Lasers Surg. Med.* **28** 113–20

Aguilar G, Verkryusse W, Majaron B, Svaasand L O, Lavernia E J and Nelson J S 2001 Measurement of heat flux and heat transfer coefficient during continuous cryogen spray cooling for laser dermatologic surgery *IEEE J. Sel. Top. Quantum Electron.* **7** 1013–21

Aguilar G, Wang G X and Nelson J S 2003 Dynamic behaviour of cryogen spray cooling: effects of spurt duration and spray distance *Lasers Surg. Med.* **32** 152–9

Beck J V, Blackwell B and St Clair CR Jr 1985 *Inverse Heat Conduction: Ill Posed Problems* (New York: Wiley)

Carslaw H S and Jaeger J C 1959 *Conduction of Heat in Solids* (London: Oxford University Press)

Choi B and Welch A J 2002 Infrared imaging of 2-d temperature distribution during cryogen spray cooling *Trans. ASME, J. Biomech. Eng.* **124** 669–75

Duck F A 1990 *Physical Properties of Tissue* (London: Academic)

Franco W, Wang G X, Karapetian E, Nelson J S and Aguilar G 2004a Effect of surface thermal variations during cryogen spray cooling in dermatologic laser therapy *Proc. ILASS Americas 17th Annual Conf. on Liquid Atomization and Spray Systems*

Franco W, Wang G X, Nelson J S and Aguilar G 2004b Radial heat transfer dynamics during cryogen spray cooling *Proc. ASME International Mechanical Engineering Congress & Exposition* IMECE2004-59609

Incropera F P and Dewitt D P 1996 *Fundamentals of Heat and Mass Transfer* (New York: Wiley)

Karapetian E 2002 Influence of cryogenic spray parameters on surface heat extraction on human skin *Master's Thesis Department of Chemical Engineering and Materials Science* (Irvine, CA: University of California)

Meyers G E 1971 *Analytical Methods in Conduction Heat Transfer* (New York: McGraw-Hill)

Nelson J S, Milner T E, Anvari B, Tanenbaum B S, Kimel S, Svaasand L O and Jacques S L 1995 Dynamic epidermal cooling during pulsed-laser treatment of port-wine stain - a new methodology with preliminary clinical evaluation *Arch. Dermatol.* **131** 695–700

Özişik M N 1980 *Heat Conduction* (New York: Wiley)

Pennes H H 1948 Analysis of tissue and arterial blood temperature in resting human forearm *J. Appl. Physiol.* **1** 93–122

van Gemert M J C and Welch A J 1989 Time constants in thermal laser medicine *Lasers Surg. Med.* **9** 405–21

Verkruysse W, Majaron B, Aguilar G, Svaasand L O and Nelson J S 1999 Dynamics of cryogen deposition relative to heat extraction rate during cryogen spray cooling *Proc. SPIE* **3907** 37–48